Surface-enhanced magnetic moment and ferromagnetic ordering of Mn ultrathin films on fcc Co(001)

W. L. O'Brien
Synchrotron Radiation Center, University of Wisconsin–Madison, 3731 Schneider Drive, Stoughton, Wisconsin 53589

B. P. Tonner
Synchrotron Radiation Center, University of Wisconsin–Madison, 3731 Schneider Drive, Stoughton, Wisconsin 53589
and Department of Physics, University of Wisconsin–Milwaukee, 1900 East Kenwood Boulevard, Milwaukee, Wisconsin 53211
(Received 14 February 1994)

We have grown ultrathin films of Mn on fcc Co(001) substrates and have investigated their magnetic properties using the element-specific techniques of soft-x-ray absorption (SXA) and x-ray magnetic circular dichroism (XMCD). We find that a one monolayer film of Mn is ferromagnetically ordered at room temperature and magnetically aligned with the fcc Co (001) substrate. The absorption spectrum of monolayer Mn is in excellent agreement with calculations for an isolated high-spin atom. By comparing our XMCD and SXA results, we conclude that the surface layer of Mn is in a high-spin state. The ferromagnetic ordering of monolayer Mn results from this high-spin layer being in direct contact with the ferromagnetic Co substrate.

One motivation for the study of the magnetic properties of ultrathin films is the possible existence of enhanced local magnetic moments at interfaces and surface, which could lead to ferromagnetic ordering of unusual materials or artificial structures. Examples of searches for enhanced surface moments include experimental investigations of fcc Fe/Cu(001),[1,2] Co/Pd multilayers,[3] and the $c(2\times2)$ Mn/Cu(001) surface alloy,[4] as well as theoretical investigations of $c(2\times2)$ Mn/Cu(001),[5,6] the bcc Ni/Fe interface,[7] and transition-metal surfaces.[8] While there is much evidence for enhanced magnetic moments at surfaces and interfaces, there has yet to be direct experimental evidence of a link between an enhancement in local magnetic moment and long-range ferromagnetic ordering. In this paper we use a combination of the element-specific techniques of x-ray magnetic circular dichroism (XMCD) and soft-x-ray absorption (SXA) to correlate magnetic ordering to changes in the local magnetic moment. We report results from a study of the Mn/Co(001) system, and find that the surface Mn layer has an enhanced local moment. When this surface layer is in direct contact with the ferromagnetic fcc Co(001) substrate, it is ferromagnetically ordered. This study relies directly on the capability of SXA and XMCD to measure independently the magnetic moments and ordering of the two elemental species Mn and Co. This is possible because of the large separation in energy of the L edges of the two elements, and because of the large magnitude of the XMCD effect, which makes submonolayer measurements possible.

XMCD has been rapidly established as a powerful method for investigating the element-specific magnetic ordering of ultrathin films.[9–11] In XMCD of $3d$ transition elements, the $L_{2,3}$ SXA spectrum is obtained on a magnetized sample using circularly polarized photons. The magnetic dichroism signal $\sigma_M=\sigma_+-\sigma_-$ is the difference between the SXA spectrum with the photon spin parallel (σ_+) and antiparallel (σ_-) to the sample magnetization. The average of the two spectra, $\sigma_0=\frac{1}{2}(\sigma_++\sigma_-)$, is in most circumstances identical to the linearly polarized SXA spectrum. Recently, Thole *et al.*[12] and Carra *et al.*[13] have derived sum rules which relate the integrated intensity of the dichroism signal σ_M at the L_3 and L_2 edges to the ground-state expectation values $\langle L_Z\rangle$ and $\langle S_Z\rangle$ for atoms, but the application of these sum rules to solids exhibiting band ferromagnetism is still controversial.[14] For this study we need only rely on the direct proportionality between σ_M and the net vector magnetization of the sample; that is $\sigma_M\sim\boldsymbol{\Sigma}\cdot\mathbf{M}$, where $\boldsymbol{\Sigma}$ is the photon spin and $\mathbf{M}$ is the net sample magnetization.

The fcc Co(001) substrate was grown epitaxially on a Cu(001) single crystal. The Cu(001) was cleaned by repeated cycles of argon-ion bombardment and annealing to 1000 K, which produces a very sharp (1×1) low-energy electron diffraction (LEED) pattern, with spot sizes at the instrumental limit. The Co was evaporated from a high-purity (99.995%) wire. Typically ≈8–10 monolayer (ML) of Co were deposited to reduce any Cu diffusion to the surface. The Mn was evaporated from an Al_2O_3 crucible at a rate of ≈1 ML in 5 min. The Mn evaporation rate was determined by monitoring the intensity of the $c(2\times2)$ low-energy electron diffraction (LEED) spots formed at $\frac{1}{2}$ ML coverage of Mn on Cu(001).[5] The deposition rate was checked throughout the experiment using a quartz microbalance that could be placed at the sample location. Cross checking of the deposited film thicknesses was done by comparing the x-ray photoelectron spectrum (XPS) peak-height ratios, and by measuring the relative x-ray-absorption L-edge intensities, as a function of deposition time. The latter (SXA)

0163-1829/94/50(5)/2963(7)/$06.00

experiments were calibrated by measuring L-edge absorption in structured "wedge" samples with known layer thicknesses. We estimate the accuracy of our film thicknesses to be within 20%. All depositions as well as measurements were performed at room temperature. The base pressure of the vacuum chamber was 5×10^{-11} Torr, and the pressure during evaporation was 2×10^{-10} Torr. Sample cleanliness was monitored throughout the experiment by core-level photoemission which showed no oxygen or carbon contamination.

The growth mode of Co on Cu(001) at room temperature has been studied by x-ray photoelectron diffraction (XPD),[15] reflection high-energy electron diffraction (RHEED), and CO titration.[16] Li and Tonner,[15] using XPD, found that Co grows epitaxially in the fcc structure on Cu(001), with a nearly layer-by-layer growth mode after 2 ML. This was later confirmed by Kief and Egelhoff[16] who also found, through RHEED analysis, that the layer-by-layer growth mode after 2 ML continued to 10 ML. They also determined the amount of substrate Cu-atom diffusion through the cobalt film to the surface, and found that this approaches zero after 6 ML of Co deposition at room temperature. For these reasons, we selected Co films of 8–10-ML thickness for our substrates. The LEED pattern of the deposited substrate showed a very sharp (1×1) pattern.

We are not aware of any growth mode investigations for Mn deposition on fcc Co(001). However, our LEED experiments show that the substrate (1×1) spots remain up to a few ML coverage but that the background intensity grows constantly with coverage. This suggests that the Mn film does not sustain lateral coherent epitaxy with the substrate Co, but rather relaxes to a bulk Mn-Mn nearest-neighbor distance. The structure of Mn grown on other, related substrates with similar lattice mismatch suggests that Mn grows in tetragonal structures (fct or bct) on (100) surfaces. We did not find evidence of formation of the $c(2\times2)$ surface alloy (present in both Mn on Cu and Ni) with Mn on Co(001).

The SXA and XMCD experiments were performed on the 10M toroidal grating monochromator beamline located at the Synchrotron Radiation Center of the University of Wisconsin. The beamline is equipped with a water-cooled copper aperture which allows the selection of either linear, left-handed or right-handed elliptically polarized photons, with polarization of $85\pm5\%$ as determined by calculations and comparison to other XMCD work.[17] Due to the exceptional stability of the photon flux and polarization at the SRC beamline, dichroism measurements with very high reproducibility are obtained by maintaining a constant incident photon spin direction and measuring σ_+ and σ_- by reversing the sample magnetization. The reliability of this method has been checked explicitly by measuring nonferromagnetic Mn on ferromagnetic Fe, which shows that absolute XMCD intensities as small as 1% can be detected.[17]

After growth, the samples were magnetized under UHV conditions by a 2-KG electromagnet, with the field either perpendicular to the surface or in plane along any chosen axis. All XMCD measurements were made on the remnant sample magnetization at room temperature, in a chamber with a background pressure of 6×10^{-11} Torr. For in-plane magnetization measurements the incident photon beam was directed at 65° from the sample normal. The absorption spectra were measured using total electron yield $Y(\hbar\omega)$, which is related to the absorption cross section according to the relation $Y(\hbar\omega)\propto\hbar\omega\sigma(\hbar\omega)$. The yield spectra were corrected for the incident photon flux on the sample and the linear $\hbar\omega$ dependence using a Au photodiode current, normalized according to the tabulated Au photoyield.[18] This result was confirmed using a Cu diode. A linear background was subtracted from the Mn and Co $L_{2,3}$ spectra to remove the contribution from the substrate.

In Fig. 1 we show the Co $L_{2,3}$ SXA spectra (σ_+ and σ_-) obtained from an 8-ML Co film after deposition of 1 ML of Mn. Magnetization was parallel to the surface along the ⟨110⟩ direction. These spectra are shown with minimal manipulation, incorporating only a normalization to the incident photon flux. No corrections or alterations for incomplete photon polarization, smoothing, or energy shifts are needed, and none have been applied. The difference between these spectra, the XMCD spectrum σ_M, is shown on the bottom of Fig. 1. The Co film dichroism spectrum is characterized by two asymmetric peaks of opposite sign at L_3 and L_2 edges. The relative areas of the two peaks are far from the value of 1:1 expected for purely statistical branching ratios, and there is substantial intensity at the high-energy side of both the L_3 and L_2 edges, which is not correctly described by single-particle band-structure calculations. The linear polarization SXA spectrum was found to be identical to the average of the two circularly polarized spectra shown in Fig. 1.

Several extensive tests of the experimental techniques used to record XMCD spectra have been completed to eliminate systematic errors, and will be reported in detail elsewhere. We explicitly tested our method of using a

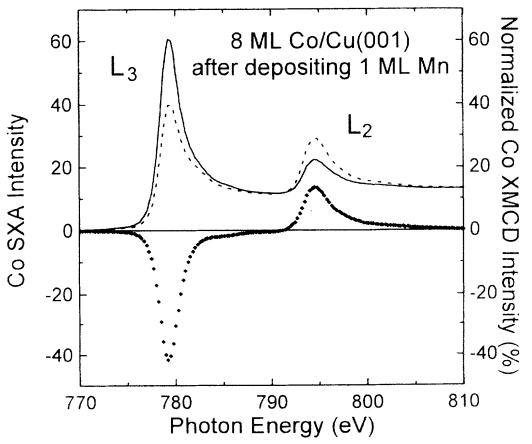

FIG. 1. (Top) Co $L_{2,3}$ soft x-ray-absorption spectra for an 8-ML film of Co after Mn deposition, obtained with circularly polarized photons: σ_+, dashed line; and σ_-, solid line. (Bottom) The difference between σ_+ and σ_- is the dichroism signal, σ_M. The sample is magnetized parallel to the surface plane along the ⟨110⟩ direction.

fixed incident polarization to measure the XMCD signal by reversing sample magnetization, with (separately) both left- and right-handed polarized light, obtained by using either the upper or lower portion of the x-ray beam (a total of four SXA spectra). The excellent agreement in the XMCD spectrum for left- and right-handed polarization is shown in Fig. 2. We also directly determined the influence of the incident photon absorption length, and outgoing secondary electron sampling depth, by a series of experiments on samples with known film thickness and varying incident photon angle. In order to correctly account for systematic errors in the measurement, it is necessary to determine the effective sampling depth, or escape depth, of the secondary electrons that make up the total electron yield. This was accurately accomplished by measuring the yield of Ni and Co in a calibrated wedge sample, consisting of a 50-Å-thick Ni underlayer, covered by a 0–30-Å Co wedge. The intensity of the SXA spectra is shown in Fig. 3, along with exponential fits for secondary electron escape depths of about 20 Å. Using the measured secondary electron sampling depths, and published photon absorption lengths, we found that the systematic error in the reported dichroism branching ratios due to absorption effects is 10% or less. A detailed experimental study of the thickness and angle-of-incidence dependence of dichroism branching ratios, which is in good agreement with the model used to analyze the data presented here, will be published elsewhere.[19]

All our magnetic studies were performed on samples at room temperature. The absolute value of the XMCD intensity at the L_3 edge can be used to monitor the degree of long-range magnetic ordering. The normalized XMCD intensity is defined as the differential absorption, divided by the linear absorption intensity at the L_3 edge maximum $\sigma_M(\hbar\omega)/\sigma_0(L_3)$. In Fig. 4 we plot $|\sigma_M(L_3)/\sigma_0(L_3)|$ obtained for different coverages of cobalt with parallel magnetization. Below 2 ML, no XMCD signal is found, in complete agreement with earlier studies that find no ferromagnetic order below 2 ML at room temperature.[20–22] These films had zero perpendicular remanence for these thicknesses at room temperature. Also in Fig. 4 is a plot of the linear polarization SXA L_3/L_2 intensity ratio for Co, as a function of film thickness. This ratio $R_0=I(L_3)/I(L_2)$ is found to be essentially constant, which will be discussed below in comparison to Mn.

In Fig. 5 we show the Mn $L_{2,3}$ σ_+, σ_-, and σ_M spectra for the same sample as in Fig. 1. These spectra are similar in that they show a negative XMCD signal at the L_3 edge and a positive signal at the L_2 edge. Due to the cosine dependence of the XMCD signal on the relative direction of the photon spin and sample magnetization

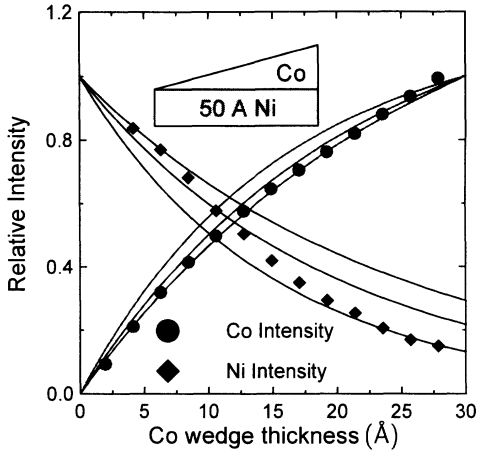

FIG. 3. Soft x-ray-absorption edge intensity from a 50-Å-thick Ni substrate covered by a 0–30-Å-thick Co wedge, used to determine the effective sampling depth (or escape depth) of secondary electrons in total yield. The curves are exponential model calculations, which assume effective depths of 15, 20, and 25 Å.

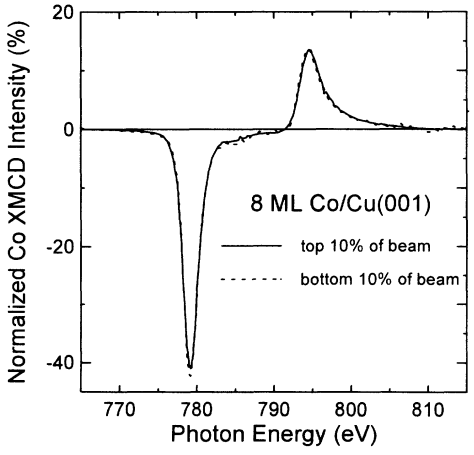

FIG. 2. Comparison of circular dichroism signal from a fcc Co(001) film using (separately) right- or left-handed circular polarization, obtained using light above or below the orbital plane. Each polarization was used to measure SXA spectra with sample magnetization parallel and antiparallel to the photon spin. The two different helicity measurements are virtually indistinguishable.

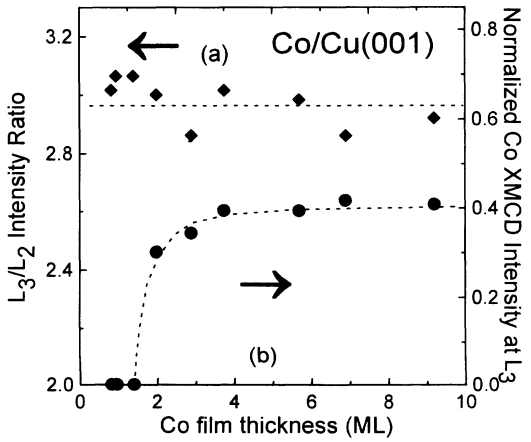

FIG. 4. Magnitude of the linear x-ray-absorption intensity ratio R_0 (a), and of the magnetic dichroism signal σ_M (b), as a function of film thickness for the fcc Co(001) substrate. The onset of ferromagnetic order is at 2 ML at room temperature.

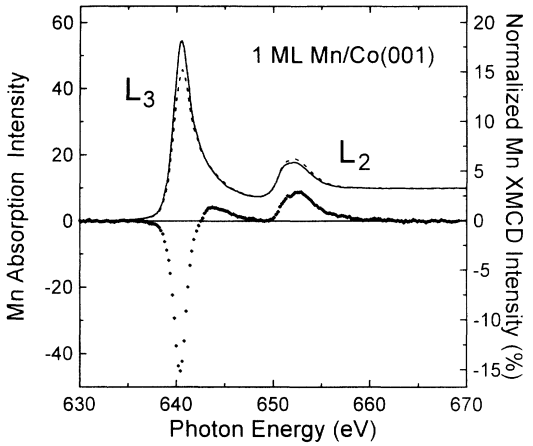

FIG. 5. (Top) Mn $L_{2,3}$ soft x-ray-absorption spectra for same sample as shown in Fig. 1, obtained with circularly polarized photons: σ_+, dashed line; and σ_-, solid line. (Bottom) The difference between σ_+ and σ_- is the magnetic dichroism spectrum σ_M (XMCD). The Mn in the 1-ML film is ferromagnetically ordered and aligned with the ferromagnetic Co substrate.

($\mathbf{\Sigma}\cdot\mathbf{M}$), we can directly infer from this result that one ML of Mn on Co(001) is magnetically ordered and ferromagnetically coupled to the Co substrate. In Fig. 6 we show the Mn $L_{2,3}$ σ_+, σ_-, and σ_M spectra for a 3-ML Mn sample. No magnetic order is found for Mn in the 3-ML film, while the underlying Co film remains magnetically ordered.

The Mn dichroism line shape differs from that of Co in a number of ways. The normalized MCD intensity is smaller for the Mn film than for the Co substrate, which is most likely due to a reduced remanence in the Mn layer. This can be determined in a future experiment with a field applied during the MCD measurement, and by varying the substrate temperature. The Mn L_3 edge dichroism also shows a different type of asymmetry from

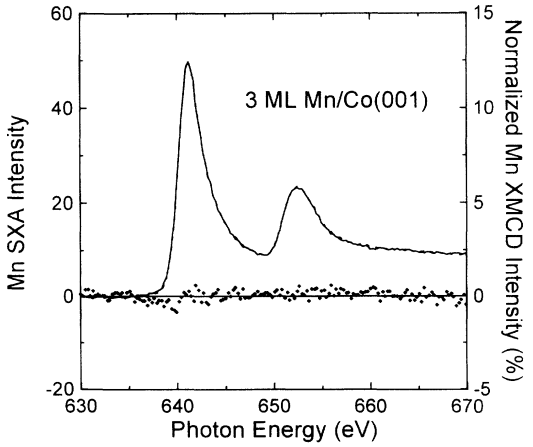

FIG. 6. (Top) Mn $L_{2,3}$ SXA spectra for 3-ML Mn/Co(001), obtained with circularly polarized photons: σ_+, dashed line; and σ_-, solid line. (Bottom) The dotted curve shows the negligible magnetic dichroism signal in this sample. Mn in a 3-ML film is not ferromagnetically ordered at room temperature.

that of Co, with the signal reversing sign after the negative intensity maximum. This is due to a trend in the periodic series (V to Ni) in which the post-L_3 edge dichroism intensity goes from negative (Ni) to near zero (Fe) to positive (Cr, Mn, and V).[19] The dichroism L_3/L_2-integrated intensity branching ratio is also very different for Co and Mn.

The absolute value of the XMCD intensity at the L_3 edge can be used to monitor the degree of long-range magnetic order in the Mn film. In Fig. 7 we plot the normalized Mn L_3 XMCD intensity $|\sigma_M(L_3)/\sigma_0(L_3)|$ obtained for different coverages of Mn. Below 2-ML coverage we find a nonzero σ_M signal. Above 2 ML we detect no σ_M signal, signifying no ferromagnetic ordering of Mn above 2 ML. The transition from magnetically ordered to nonmagnetic behavior of the Mn film is very abrupt as a function of film thickness. The data in Fig. 7 are compared to three elementary models which assume different magnetic ordering behavior. The model is based on an incoherent addition of the XMCD signal expected from each layer of a multilayer Mn film, assuming that the amplitude of an individual layer is given by the measured monolayer signal, and that the total-electron-yield sampling depth is much larger than the film thickness. The first growth model, represented by the dash-dot line, assumes that the first monolayer of Mn remains in a ferromagnetic state, and the subsequent overlayers are magnetically disordered. The intensity of the normalized σ_M signal at 4 ML, according to this model, is simply $\frac{1}{4}$ of that at 1 ML. This model clearly does not fit the data.

Another possible growth mode of Mn is antiferromagnetic ordering, in which each layer is magnetized in-plane but opposite in direction to neighboring layers. This

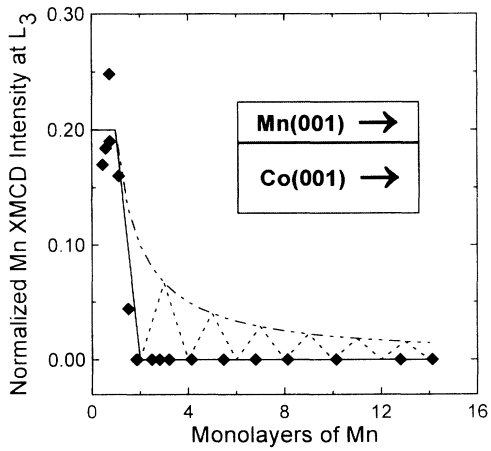

FIG. 7. Normalized Mn $L_{2,3}$ XMCD intensity (σ_M/σ_0 measured at the L_3 peak) vs film thickness. The dichroism intensity abruptly drops to zero at 2-ML coverage. The experimental results are compared to three models assuming different magnetic ordering behavior: (1) Only the Mn at the Co/Mn interface is ferromagnetically ordered and remains ordered for thicker coverage, dash-dot line. (2) Mn grows antiferromagnetically in a layer-by-layer mode, dotted line. (3) The Mn at the Co/Mn interface is ferromagnetically ordered but only when it is also on the surface, solid line.

magnetic ordering sequence has been proposed to explain spin-resolved electron scattering data for the growth of Mn on Fe(001).[23] The dotted line in Fig. 7 represents this model. If instead of growing layer by layer (which is unlikely in the present case) there is three-dimensional islanding (Volmer-Weber growth) with antiferromagnetic ordering, the model curve would assume a form similar to the shape of a decaying exponential, as has been proposed to explain the XMCD data from Cr films.[24] Because of the accuracy with which the absolute coverage is known, and the limits placed on the amount of exposed substrate by XPS and SXA intensity ratios as a function of coverage, the three-dimensional islanding model is in poor agreement with our data for reasonable estimates of possible island heights at low coverage. A further argument against antiferromagnetic layering is that, in cases for which it has been observed (Mn/Fe,[23] Cr/Fe[24]), the first layer is antiferromagnetically aligned with the substrate. In Mn/Co, the alignment is ferromagnetic.

In the third model, represented by the solid line, the first ML of Mn is assumed to be ferromagnetically ordered but only when it is also on the surface, in a low-coordination site. Once the Mn/Co interface layer is covered with additional Mn it becomes magnetically disordered. This model is the only one of the three which can explain the extremely abrupt transition from magnetically ordered to magnetically disordered over a range of thickness of only one monolayer, from 1- to 2-ML thickness.

In addition to the direct information about long-range magnetic ordering we obtain from the dichroism intensity, there is also information available about the local magnetic properties of the linear (or polarization averaged) SXA spectra. The average of the right- and left-handed spectra, in most cases, are equivalent to the linear absorption spectrum, and this was checked explicitly for these experiments. The branching ratio of the L_3 and L_2 edges in the linearly polarized SXA spectrum of Mn can be used to detect changes in the local magnetic moment. This is accomplished by correlating the SXA branching ratio with the ground-state spin, by reference to theoretical calculations. The validity of the comparison is verified by showing a close agreement between the experimental SXA spectrum for Mn and the corresponding calculation.

In Fig. 8 we show the x-ray-absorption spectrum (σ_0) of 1.0 ML of Mn, in comparison to the theoretical calculation of high-spin atomic Mn d^5, $S=\frac{5}{2}$. The theoretical spectrum was rigidly shifted along the photon energy axis to align the L_3 peaks. The atomic spectrum matches the experimental spectrum quite well, reproducing the broad doublet of the L_2 peak, and the intensity ratio of the L_3 and L_2 lines. We note that similar agreement has been found for Mn in dilute AgMn and CuMn alloys, where dilute Mn is known to have a high magnetic moment in these noble metals.[26] This agreement between experiment and theory is particular to a 1-ML film. For example, in Fig. 9 we show the Mn $L_{2,3}$ σ_0 spectra for three different coverages of Mn. The spectra have all been normalized to have the same integrated L_2 intensity. It is quite apparent that the relative intensity of the L_3 line is

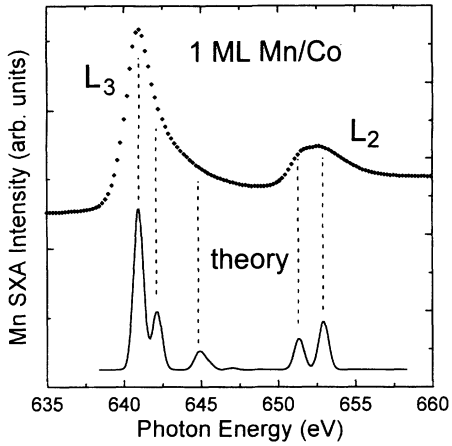

FIG. 8. Mn $L_{2,3}$ SXA spectra σ_0 compared to atomic calculations on high-spin Mn d^5, $S=\frac{5}{2}$ (Ref. 25). The comparison is good, especially noting the doublet structure of the L_2 peak, and the intensity ratio $I(L_3)/I(L_2)$. This suggests that the first ML of Mn on Co(001) is in a high-spin state.

reduced for thicker coverages. In addition, the L_2 peak becomes sharper, and does not appear to be a doublet, for higher coverages (see the inset of Fig. 9).

We now consider the large change in the L_3/L_2 intensity ratio R_0 vs film thickness. Thole and van der Laan[25] have shown that R_0 is larger for high-spin ground states in atoms. This has been verified by experiment on FeGe alloys,[27] Fe compounds,[25] dilute Mn alloys,[26] and Mn surface alloys.[4] In Fig. 10 we plot the Mn $L_{2,3}$ linear intensity ratio R_0 vs film thickness. R_0 is obtained by integrating the L_3 peak between photon energies of 637–648 eV, and the L_2 peak between photon energies of

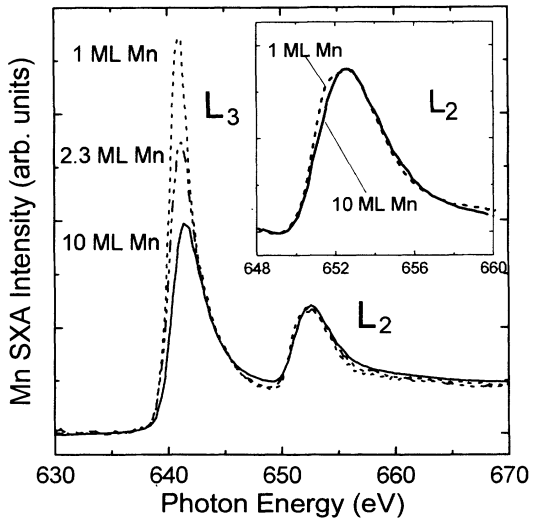

FIG. 9. Mn $L_{2,3}$ SXA spectra σ_0 for different Mn coverages. The spectra have been normalized to the integrated L_2 intensity. The intensity ratio $R_0=I(L_3)/I(L_2)$ is greatly reduced for thicker films implying a reduction in local magnetic moment. (Inset) Details of the L_2 peak for 1- and 10-ML-thick films. For the thicker film, the L_2 peak is sharper and does not appear as a doublet.

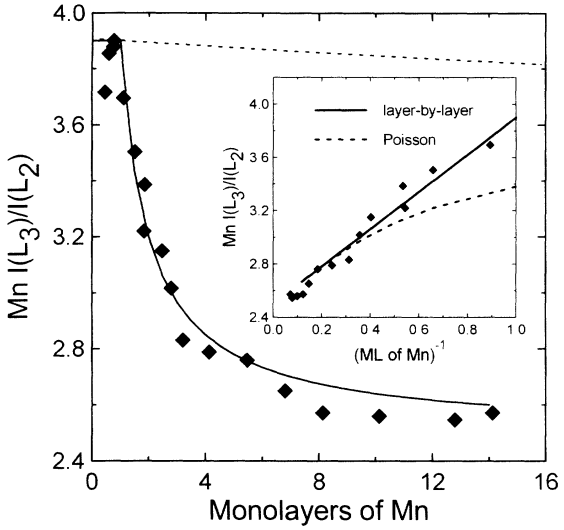

FIG. 10. Mn L-edge intensity ratio $R_0 = I(L_3)/I(L_2)$ vs film thickness. The solid line represents a parameterless model which assumes that 1 ML of Mn has a large local magnetic moment, and that the remaining Mn has the local magnetic moment of bulk Mn. The dashed line is the calculated upper bound to the change in R_0 due to experimental artifacts (see text). (Inset) Intensity ratio plotted vs inverse film thickness. The solid line assumes ideal layer-by-layer growth, and the dashed line is for a Poisson distribution three-dimensional growth mode.

648–659 eV, using a linear background between the endpoints of integration. R_0 drops off quickly after 1-ML coverage, approaching a value of 2.5 after about 10 ML. This data are compared to a simple model which assumes that a Mn film of n ML thickness consists of 1 ML of high-spin Mn and $(n-1)$ ML of low-spin Mn, where R_0 for high- and low-spin Mn are taken from the experimental data for 1- and 14-ML coverages, respectively. The change in branching ratio with coverage is very well described by this model, which has no free parameters.

We have calculated the expected thickness dependence of the intensity ratio for nonideal growth modes as well. Specifically, we assume that the film thickness follows a Poisson distribution, and the limiting intensity ratios are taken directly from the data for low and high coverage. This is again a parameter-free model. The inset to Fig. 10 shows the measured intensity ratio as a function of inverse coverage, compared to a layer-by-layer growth mode model (solid line), and the Poisson distribution model (dashed line). There is clearly a much better match to the layer-by-layer model than to the three-dimensional growth (Poisson) model. We have also developed models which assume a more complicated magnetic structure in the Mn films. In these models the magnetic moment of each monolayer can be different. These models are similar to those recently proposed for the magnetism in thin films of Cr on Fe.[28] The fit to the experiment is only slightly improved using these more complicated models. The assumption of a single high-spin layer appears to be accurate. There may be variations in the moment of other layers, but these variations are much smaller than the change at the high-spin layer.

Before discussing these results in greater detail, we elaborate on the possible effects of experimental artifacts. It is known that total yield measurements are not strictly proportional to the sample absorption. If the penetration depth of the photon is not much greater than the escape depth of the secondary electrons, the relative intensity of the most intense features will be reduced. This experimental artifact has been termed saturation, since it results in observed absorption peak intensities that are smaller than the true value. It can lead to a change in the intensity ratio R_0 as a film thickness increases that is only an artifact due to saturation. We have performed test experiments and calculations to determine the magnitude of this effect in our study.

The total electron yield $Y(\hbar\omega)$ can be written

$$Y(\hbar\omega) \propto \frac{\sigma(\hbar\omega)\hbar\omega}{\cos\theta} \int_0^d e^{-z\{(1/\lambda_e)+[\sigma(\hbar\omega)\rho/\cos\theta]\}} dz \ , \qquad (1)$$

for a homogeneous film of thickness d. Here σ is the absorption cross section, θ the angle of incidence of the photon beam, ρ the atomic density, and λ_e the detection depth for total electron yield (the effective escape depth of secondary electrons). The extension of this formula to nonhomogeneous films is straightforward, as it simply introduces a depth dependence to the cross section σ and atomic density ρ. We have calculated the effects of saturation on R_0 using (1) and assuming $\lambda_e = 20$ Å, based on our measurements in Fig. 3. To approximate σ we use the Mn σ_0 spectra obtained for a 1-ML film, since $Y(\hbar\omega) \propto \hbar\omega\sigma(\hbar\omega)$ in the zero-thickness limit. This spectrum was normalized using total atomic cross-section calculations.[29] Using this procedure, the cross sections at the L_3 peak maximum and just before the L_3 peak were assumed to be 3.2 and 0.2 Mb, respectively. The results of this calculation are shown in Fig. 10 as the dashed line. Saturation causes a very minor ($<3\%$) change in R_0 for films in this thickness range. We further note that saturation would flatten out peaks for thicker film thickness, which is opposite to the sharpening of the L_2 peak in thicker Mn films that we observe, Fig. 9.

The change in intensity ratio R_0 from Mn, as shown in Figs. 9 and 10, is a very large effect. Usually, changes in the SXA spectra of metals of this order of magnitude are associated with gross changes in chemical state. In these samples, however, the changes are due only to changing the coordination of the Mn atom from a surface atom to a bulk atom. If we take the value of R_0 for the monolayer as being that of purely high-spin Mn, and the value for the 15-ML film to be purely low spin, then the magnitude of the high- and low-spin intensity ratios are in qualitative agreement with calculations for isolated Mn d^5 atoms by Thole and van der Laan.[25] We believe the agreement between theory and experiment for R_0 of the 1-ML film is not fortuitous. This is based on the close agreement to atomic theory, Mn $d^5 S = \frac{5}{2}$, of the 1-ML Mn/Co absorption spectra. The spin in the 1-ML film is near the maximum possible for d electrons, $S = \frac{5}{2}$. The agreement between bulk R_0 for experiment and theory is probably fortuitous. Valence mixing for bulk Mn atoms,

due to the increased coordination, will introduce d^4 and d^6 character and a variety of spin states. The spin moment of these states must be less than the moment in the 1-ML film. The low-spin d^5 state probably has a very low weight in the ground state.

The results in Fig. 10 establish that a high-spin layer of Mn is present in the Mn films. This high-spin layer should either be at the Mn/Co interface or on the surface. The enhancement in the Mn moment at a buried interface depends on the reduction of the Mn bandwidth due to the interface. We assert that a greater reduction in bandwidth will occur at the surface. This is consistent with magnetic-moment calculations of 1- and 2-ML films of Fe grown on Cu(001).[30] The moment in the Fe layer on the surface is $2.85\mu_B$ for both the 1- and 2-ML films while the moment at the buried interface is $2.6\mu_B$. Also, if the high-spin layer was fixed at the Mn/Co interface, we would expect to see ferromagnetic behavior for films thicker than 2 ML. Since we clearly do not find this (see Fig. 7), it must be the surface layer which has a high magnetic moment. It is reasonable to assume that the high-spin layer is on the surface since the reduced coordination can lead to a magnetic moment of surface atoms that is enhanced relative to the bulk value.[8]

We also find that the enhanced surface moment model, tested in Fig. 10, gives support to our preferred model describing the ferromagnetic ordering of Mn on Co. A 1-ML film of Mn on Co has a high local magnetic moment. Since it is in direct contact with the ferromagnetic Co the high-spin Mn is aligned ferromagnetically. Thicker films still have surface Mn atoms in a high-spin ground state, but they are not coupled directly to the Co. The Mn at the interface in these thicker films has a smaller local magnetic moment and is not ferromagnetically aligned. It is the enhanced magnetic moment of surface Mn atoms and the direct coupling to the ferromagnetic substrate that is responsible for the ferromagnetic ordering of 1 ML of Mn on fcc Co(001).

We believe this is the first example of a large branching ratio change observed in an elemental sample as a function of film thickness. We have seen similar effects in other systems which have been predicted to have enhanced surface moments, such as Mn/Cu(100),[4] Mn/Ni(100), Mn/Fe(100), and Mn/Ir(111),[19] but not in systems for which theory predicts very small moment enhancement,[8] for example the Co/Cu(001) sample reported here [Fig. 4(a)]. We find that subsurface Mn atoms do not have enhanced moments, so that Mn films that are "capped" by additional overlayers, or Mn layers in sandwich structures and superlattices, will not exhibit the enhanced surface moment. This experimental approach, which combines measuring local moments as reflected in the linearly polarized branching ratio with measuring long-range ordering with circular polarization, is applicable to a number of transition-metal epitaxial film systems. An important future experiment is to measure the XMCD as a function of temperature, to determine the nature of the magnetic coupling of the Co substrate and Mn monolayer.

This work was supported by the National Science Foundation, Division of Materials Research under Grant No. DMR-91-15987. The Synchrotron Radiation Center is a national facility supported by the NSF Division of Materials Research.

[1]J. Thomassen, F. May, B. Feldman, M. Wuttig, and H. Ibach, Phys. Rev. Lett. **69**, 3831 (1992).
[2]J. G. Tobin, G. D. Waddill, and D. P. Pappas, Phys. Rev. Lett. **68**, 3642 (1992).
[3]Y. Wu, J. Stöhr, B. D. Hermsmeirer, M. G. Samant, and D. Weller, Phys. Rev. Lett. **69**, 2307 (1992).
[4]W. L. O'Brien, J. Zhang, and B. P. Tonner, J. Phys. Condens. Matter **5**, L515 (1993).
[5]M. Wuttig, Y. Gauthier, and S. Blügel, Phys. Rev. Lett. **70**, 3619 (1993).
[6]M. Wuttig *et al.*, Phys. Rev. B **48**, 12 082 (1993).
[7]J. I. Lee, S. C. Hong, A. J. Freeman, and C. L. Fu, Phys. Rev. B **47**, 810 (1993).
[8]O. Eriksson, A. M. Boring, R. C. Albers, G. W. Fernando, and B. R. Cooper, Phys. Rev. B **45**, 2868 (1992).
[9]C. T. Chen, F. Sette, Y. Ma, and S. Modesti, Phys. Rev. B **42**, 7262 (1990).
[10]G. Schutz, W. Wagner, W. Wilhelm, P. Kienle, R. Zeller, R. Frahm, and G. Materlik, Phys. Rev. Lett. **58**, 737 (1987).
[11]Y. U. Idzerda, L. H. Tjeng, H.-J. Lin, C. J. Guitierrez, G. Meigs, and C. T. Chen, Phys. Rev. B **48**, 4144 (1993).
[12]B. T. Thole, P. Carra, F. Sette, and G. van der Laan, Phys. Rev. Lett. **68**, 1943 (1992).
[13]P. Carra, B. T. Thole, M. Altarelli, and X. Wang, Phys. Rev. Lett. **70**, 694 (1993).
[14]R. Wu, D. Wang, and A. J. Freeman, Phys. Rev. Lett. **71**, 3581 (1993).
[15]H. Li and B. P. Tonner, Phys. Rev. B **40**, 10 241 (1989).
[16]M. T. Kief and W. F. Egelhoff, Phys. Rev. B **47**, 10 785 (1993).
[17]R. Hanson, W. L. O'Brien, and B. P. Tonner, Nucl. Instrum. Methods (to be published).
[18]R. Haensel, C. Kunz, T. Sasaki, and B. Sonntag, Appl. Opt. **7**, 301 (1968).
[19]W. L. O'Brien and B. P. Tonner (unpublished).
[20]P. Krams, F. Lauks, R. L. Stamps, B. Hillebrands, and G. Guntherodt, Phys. Rev. Lett. **69**, 3674 (1992).
[21]C. M. Schneider, P. Bressler, P. Schuster, J. Kirschner, J. J. de Miguel, and R. Miranda, Phys. Rev. Lett. **64**, 1059 (1990).
[22]G. J. Mankey, M. T. Kief, and R. F. Willis, J. Vac. Sci. Technol. A **9**, 1595 (1991).
[23]T. G. Walker and H. Hopster, Phys. Rev. B **48**, 3563 (1993).
[24]Y. U. Idzerda, L. H. Tjeng, H.-J. Lin, C. J. Gutierrez, F. Meigs, and C. T. Chen, Surf. Sci. **287/288**, 741 (1993).
[25]B. T. Thole and G. van der Laan, Phys. Rev. B **38**, 3158 (1988); G. van der Laan and B. T. Thole, *ibid.* **43**, 13 401 (1991).
[26]B. T. Thole, R. D. Cowan, G. A. Sawatzky, J. Fink, and J. C. Fuggle, Phys. Rev. B **31**, 6856 (1985).
[27]T. I. Morrison, M. B. Brodsky, N. J. Zaluzec, and L. R. Sill, Phys. Rev. B **32**, 3107 (1985).
[28]C. Turtur and G. Bayreuther, Phys. Rev. Lett. **72**, 1557 (1994).
[29]J. J. Yeh and I. Lindau, At. Data Nucl. Data Tables **32**, 1 (1985).
[30]C. L. Fu and A. J. Freeman, Phys. Rev. B **35**, 925 (1987).

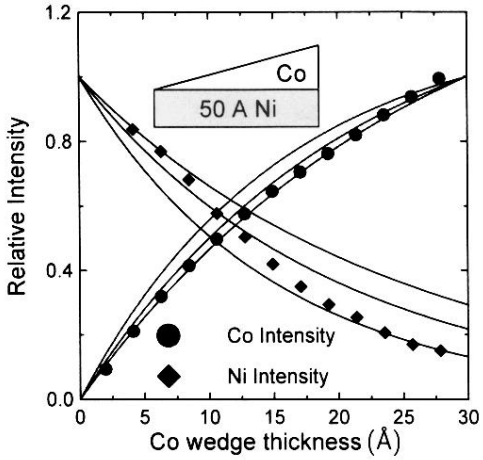

FIG. 3. Soft x-ray-absorption edge intensity from a 50-Å-thick Ni substrate covered by a 0–30-Å-thick Co wedge, used to determine the effective sampling depth (or escape depth) of secondary electrons in total yield. The curves are exponential model calculations, which assume effective depths of 15, 20, and 25 Å.